Articles

An *in Situ* X-ray Absorption Fine Structure Study of Different Oxidation States of Oxo- and Hydroxo-Bridged Ruthenium Dimers in Acetonitrile Solution

Mats Valli, Seiya Miyata, Hisanobu Wakita, and Toshio Yamaguchi*

Department of Chemistry, Fukuoka University, Fukuoka 814-80, Japan

Akihiro Kikuchi, Keisuke Umakoshi, Taira Imamura, and Yoichi Sasaki

Division of Chemistry, Graduate School of Science, Hokkaido University, Sapporo 060, Japan

Received March 21, 1997[⊗]

X-ray absorption fine structure (XAFS) experiments have been performed in acetonitrile solution with an *in situ* electrochemical cell at controlled electric potentials on $[Ru_2(\mu\text{-O})(\mu\text{-CH}_3\text{COO})_2(bpy)_2L_2]^{n+}$ (bpy = 2,2′-bipyridine; L = pyridine (**1**) and 1-methylimidazole (**2**)) with the formal ruthenium oxidation states $Ru^{II}Ru^{III}$, $Ru^{III}Ru^{III}$, and $Ru^{III}Ru^{IV}$. Spectra were also recorded for the corresponding hydroxo-bridged species, abbreviated as $Ru^{II}Ru^{II}H$, $Ru^{II}Ru^{III}H$, and $Ru^{III}Ru^{III}H$, which were formed by addition of *p*-toluenesulfonic acid to **1** and **2** and subsequent electrolysis. The X-ray absorption near edge structure (XANES) spectra all showed similar features, although a small shift toward higher threshold energy was observed with increasing formal ruthenium oxidation state. It is concluded from the analysis of the EXAFS data that the ruthenium−ruthenium distance of the μ-oxo complexes decreases with decreasing formal ruthenium oxidation state, interpreted as resulting from decreased electrostatic repulsion between the ruthenium atoms. However, for the μ-hydroxo complexes the ruthenium−ruthenium distance decreases in the order $Ru^{III}Ru^{III}H > Ru^{II}Ru^{II}H > Ru^{II}Ru^{III}H$. The present coordination structures of the oxo- and hydroxo-bridged ruthenium dimers of the different oxidation states are compared with related iron and vanadium dimers.

Introduction

Oxo- and hydroxo-bridged iron centers are common in metalloproteins such as hemerythrin, ribonucleotide reductase, and mammalian purple acid phosphatase.[1−6] These enzymes catalyze substrates in redox reactions which often involves a proton transfer. During the redox cycle the diiron metal centers have various oxidation states, among which the mixed-valence states such as $Fe^{II}Fe^{III}$ and $Fe^{III}Fe^{IV}$ are important active forms of the enzymes. Thus, structural information on the iron centers of various oxidation states is of vital importance in understanding the enzyme activation mechanism. A large number of simple iron complexes have so far been prepared to serve as models of these proteins. However, little structural information on the wide range of oxidation states is available, due to instability of the model complexes, which are usually isolated as $Fe^{III}Fe^{III}$ species, in solution. With regard to the solid-state structures of the μ-oxo−μ-carboxylato complexes, although a number of single-crystal structure determinations have been reported on the $Fe^{III}Fe^{III}$ complexes, only one structural determination has been known for the $Fe^{II}Fe^{III}$ state, namely that of $[Fe^{II}Fe^{III}(\mu\text{-OH})(\mu\text{-pivalate})_2(Me_3tacn)_2]^{2+}$ (Me_3tacn = 1,4,7-trimethyl-1,4,7-triazacyclononane).[7]

Oxo- and hydroxo-bridged dinuclear ruthenium complexes offer an alternative approach to the structural study of oxo-bridged dimetal complexes at various oxidation states formed during the redox cycle in solution, because the di-, tri-, and tetravalent ruthenium ions are all substitution inert and stable enough for a relevant study of the structure.[8−26] Among various

* To whom all correspondence should be addressed.

[⊗] Abstract published in *Advance ACS Abstracts,* September 1, 1997.

(1) Vincent, J. B.; Olivier, G. L.; Averill, B. A. *Chem. Rev.* **1990**, *90*, 1447.
(2) Lippard, S. J. *Angew. Chem., Intl. Ed. Engl.* **1988**, *27*, 353.
(3) Kurtz, D. M., Jr. *Chem. Rev.* **1990**, *90*, 585.
(4) Que, L. Jr.; True, A. E. *Prog. Inorg. Chem.* **1990**, *38*, 97.
(5) Bertini, I.; Gray, H. B.; Lippard, S.; Valentine, J. S. In *Bioinorganic Chemistry*; University Science Books: Mill Valley, CA, 1994.
(6) Lippard, S. J.; Berg, J. M. In *Principles of Bioinorganic Chemistry*; University Science Books: Mill Valley, CA, 1994.
(7) Bossek, U.; Hummel, H.; Weyhermueller, T.; Bill, E.; Wieghardt, K. *Angew. Chem., Intl. Ed. Engl.* **1995**, *34*, 2642.
(8) Sasaki, Y.; Suzuki, M.; Nagasawa, A.; Tokiwa, A.; Ebihara, M.; Yamaguchi, T.; Kabuto, C.; Ochi, T.; Ito, T. *Inorg. Chem.* **1991**, *30*, 4903.
(9) Neubold, P.; Wieghardt, K.; Nuber, B.; Weiss, J. *Angew. Chem., Intl. Ed. Engl.* **1988**, *27*, 933.
(10) Neubold, P.; Wieghardt, K.; Nuber, B.; Weiss, J. *Inorg. Chem.* **1989**, *28*, 459.
(11) Sudha, C.; Mandal, S. K.; Chakravarty, A. R. *Inorg. Chem.* **1993**, *32*, 3801.
(12) Gupta, N.; Mukerjee, S.; Mahapatra, S.; Ray, M.; Mukherjee, R. *Inorg. Chem.* **1992**, *31*, 139.
(13) Llobet, A.; Curry, M. E.; Evans, H. T.; Meyer, T. J. *Inorg. Chem.* **1989**, *28*, 3131.
(14) Syamala, A.; Chakravarty, A. R. *Inorg. Chem.* **1991**, *30*, 4699.
(15) Das, B. K.; Chakravarty, A. R. *Inorg. Chem.* **1991**, *30*, 4978.
(16) Sasaki, Y.; Suzuki, M.; Tokiwa, A.; Ebihara, M.; Yamaguchi, T.; Kabuto, C.; Ito, T. *J. Am. Chem. Soc.* **1988**, *110*, 6251.
(17) Syamala, A.; Chakravarty, A. R. *Polyhedron* **1994**, *13*, 3097.
(18) Mitchell, R. W.; Spencer, A.; Wilkinson, G. *J. Chem. Soc., Dalton Trans.* **1973**, 846.
(19) Das, B. K.; Chakravarty, A. R. *Inorg. Chem.* **1990**, *29*, 1784.
(20) Das, B. K.; Chakravarty, A. R. *Inorg. Chem.* **1990**, *29*, 2078.
(21) Barral, M. C.; Aparicio, R. J.; Royer, E. C.; Urbanos, F.A.; Monge, A.; Valero, C. R. *Polyhedron* **1991**, *10*, 113.
(22) Ochi, T.; Sasaki, Y.; Yamaguchi, T.; Ito, T. *Chem. Lett.* **1991**, 2019.

S0020-1669(97)00339-X CCC: $14.00

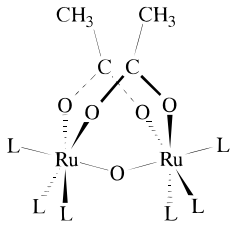

Figure 1. Structure of $[Ru_2(\mu\text{-}O)(\mu\text{-}CH_3COO)_2(bpy)_2L_2]^{n+}$ (L = pyridine, 1-methylimidazol).

Scheme 1

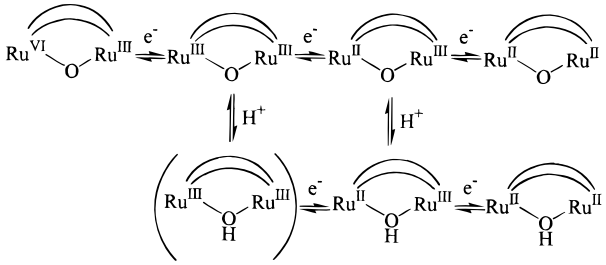

dimeric ruthenium complexes redox behaviors of the complexes $[Ru_2(\mu\text{-}O)(\mu\text{-}CH_3COO)_2(bpy)_2L_2]^{2+}$ (bpy = 2,2′-bipyridine; L = pyridine (py) (**1**), 1-methylimidazole (meim) (**2**); Figure 1) are particularly interesting since they show proton-coupled redox reactions both in acetonitrile and in aqueous media. In acetonitrile the complexes show a reversible oxidation wave for the $Ru^{III}Ru^{IV}/Ru^{III}Ru^{III}$ couple, one quasi-reversible wave for the $Ru^{III}Ru^{III}/Ru^{II}Ru^{III}$ couple, and an irreversible wave for the $Ru^{II}Ru^{III}/Ru^{II}Ru^{II}$ couple. On the addition of an equal amount of a strong acid, *p*-toluenesulfonic acid (TsOH), to the solutions, two reduction waves remarkably shift to more positive potentials with improved reversibility, which has been accounted for by protonation at the oxide bridge of the $Ru^{II}Ru^{III}$ and $Ru^{II}Ru^{II}$ states (see Scheme 1).[27]

The crystal structures for the (μ-oxo)- or (μ-hydroxo)bis(μ-carboxylato)diruthenium complexes have been determined at high oxidation states. Neubold *et al.* reported the crystal structures of $[Ru_2(\mu\text{-}O)(\mu\text{-}CH_3COO)_2(Me_3tacn)_2]^{n+}$ with $Ru^{III}Ru^{III}$ ($n = 2$) and $Ru^{III}Ru^{IV}$ ($n = 3$) and of the corresponding hydroxo-bridged $Ru^{III}Ru^{III}$.[9,10] They found a lengthening of the ruthenium−ruthenium distance from 3.258 to 3.342 Å upon oxidation of the oxo-bridged $Ru^{III}Ru^{III}$ species to $Ru^{III}Ru^{IV}$ and to 3.472 Å upon protonation of the oxo-bridge of $Ru^{III}Ru^{III}$ state. Similar structural changes have been observed for $[Ru_2(\mu\text{-}O)(\mu\text{-}CH_3COO)_2(meim)_6]^{n+}$ with the ruthenium−ruthenium distance increasing from 3.266 to 3.326 Å upon oxidation of $Ru^{III}Ru^{III}$ to $Ru^{III}Ru^{IV}$.[12] However, no oxo- or hydroxo-bridged ruthenium dimers with lower oxidation states, such as $Ru^{II}Ru^{III}$ or $Ru^{II}Ru^{II}$, has been isolated and characterized except for the crystal structure of $[Ru^{II}Ru^{III}(\mu\text{-}OH_2)(\mu\text{-}C_6H_5COO)_2Cl(MeCN)(O_2CAr)_2(PPh_3)_2]$ and $[Ru^{II}_2(\mu\text{-}OH_2)(\mu\text{-}C_6H_5COO)_2(MeCN)_2(O_2CAr)_2(PPh_3)_2]$.[15]

X-ray absorption fine structure (XAFS) spectroscopy of a sample in an electrochemical cell has been proved useful to determine local structural parameters of metal complexes at various oxidation states stabilized electrochemically in solution.[28,29] In this study we have used the XAFS technique to determine the local coordination structures of **1** and **2** in different ruthenium oxidation states in an acetonitrile solution. For this purpose an *in situ* electrochemical cell was designed that allowed for the XAFS measurements while the different oxidation states $Ru^{II}Ru^{III}$, $Ru^{III}Ru^{III}$, and $Ru^{III}Ru^{IV}$ of the samples were electrochemically stabilized. The corresponding hydroxo-bridged species, $Ru^{II}Ru^{II}H$, $Ru^{II}Ru^{III}H$ and $Ru^{III}Ru^{III}H$, were also generated by adding an equimolar amount of TsOH to the solution of **1** and **2**, and their structures were characterized and compared to those of the oxo complexes.

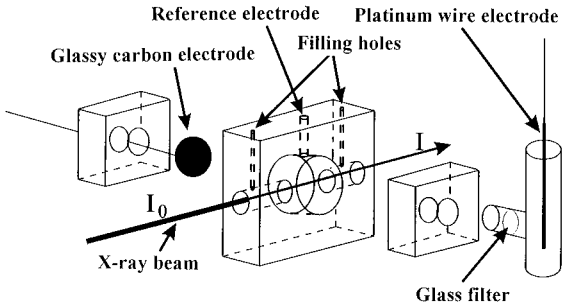

Figure 2. The *in situ* electrochemical XAFS cell.

Experimental Section

Materials. Ruthenium complexes **1** and **2** were prepared and isolated as PF_6^- salts as previously described.[8] Tetrabutylammonium hexafluorophosphate (Tokyo Kasei Kogyo, Tokyo, Japan) was recrystallized from ethanol and used as supporting electrolyte in the electrochemical experiments. *p*-Toluenesulfonic acid (TsOH, Wako Pure Chemical Industries, Ltd., Osaka, Japan) was dried at 70 °C before use. Tris(acetylacetato)ruthenium(III) and ruthenium(IV) oxide (Wako Pure Chemical Industries, Ltd.) were used as received to check the XAFS refinements. Ruthenium foil (Goodfellow Cambridge Ltd., Cambridge, Great Britain) was used as received for energy calibration. Acetonitrile was distilled over calcium hydride (CaH_2) or molecular sieves, 4 Å, under argon atmosphere prior to use.

Physical Measurements. Electrochemistry. An *in situ* electrochemical cell that allows for the electrolysis and simultaneous recording of the XAFS spectra, has been designed, Figure 2. The counter cell, made of glass, is separated from the working cell, made of Teflon, by a No. 4 glass frit. The cell windows are made of Mylar and/or Kapton. These window materials have negligible absorption at the Ru K-edge (22.120 keV). The optical path length can be varied by inserting appropriate Teflon spacers. All joints are sealed by o-rings. The cell was placed on two alignment pins on a motorized XZ-table which allowed for precise alignment of the cell with the X-ray beam.

Cyclic voltammograms were recorded by use of a Hokuto HA-501G potentiostat with a Hokuto HB-105 function generator and a Graphtec WX2400 XY-recorder. Glassy carbon and platinum electrodes were used as working and counter electrodes, respectively. The samples (20 mM) were dissolved in an acetonitrile solution containing 0.5 M tetrabutylammonium hexafluorophosphate, $(TBA)PF_6$, and the solutions were deoxygenated by a stream of nitrogen or argon gas. The scan rate was 50 mV s^{-1}. An Ag/AgCl electrode, against which the half-wave potential of ferrocene/ferrocenium was +0.44 V, was used as a reference. Controlled potential coulometry was performed on the same solution by using a Hokuto HA-310 potentiostat and a Hokuto HF-201 coulometer.

XAFS Measurements. Ruthenium K-edge EXAFS spectra were recorded at the unfocused bending magnet beam line 10B in the Photon

(23) Syamala, A.; Das, B. K.; Chakravarty, A. R. *Polyhedron* **1992**, *11*, 335.
(24) Syamala, A.; Chakravarty, A. R. *Polyhedron* **1993**, *12*, 273.
(25) Barral, M. C.; Aparicio, R. J.; Kramolowsky, R.; Wagner, I. *Polyhedron* **1993**, *12*, 903.
(26) Kahn, M. M. T.; Hussain, A.; Moiz, M. A.; Chatterjee, D.; Thorat, R. B. *Polyhedron* **1993**, *12*, 1437.
(27) (a) Kikuchi, A.; Fukumoto, T.; Umakoshi, K.; Sasaki, Y.; Ichimura, A. *J. Chem. Soc., Chem. Commun.* **1995**, 2125. (b) Imamura, T.; Kishimoto, A.; Sumiyoshi, T.; Takahashi, K.; Fukumoto, T.; Sasaki, Y. *Bull. Chem. Soc. Jpn.* **1995**, *68*, 3365.
(28) Sharpe, L. R.; Heineman, W. R.; Elder, R. C. *Chem. Rev.* **1990**, *90*, 705.
(29) Yamaguchi, T.; Mitsunaga, T.; Yoshida, N.; Wakita, H.; Fujiwara, M.; Matsushita, T.; Ikeda, S.; Nomura, M. *Jpn. J. Appl. Phys.* **1993**, *32*, 533.

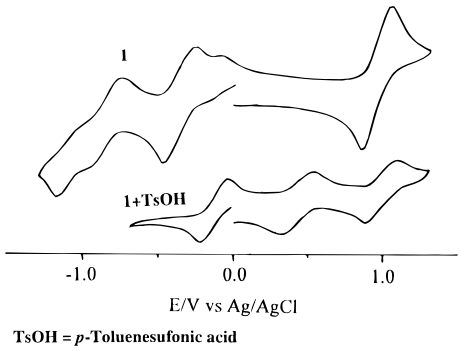

Figure 3. Cyclic voltammograms of **1** and **1** + TsOH. The scan rate was 50 mV s^{-1}, and an Ag/AgCl electrode was used as reference.

Factory (KEK, Tsukuba, Japan) under dedicated conditions, 2.5 GeV and 280−350 mA.[30,31] Monochromatic radiation was obtained by a channel-cut Si(311) monochromator. Two ion chambers with flowing argon and krypton for I_0 and I, respectively, were used as detectors. External calibration was used, assigning the first inflection point in the Ru K-edge of ruthenium foil to 22.120 keV. Since the XAFS beamlines at the Photon Factory do not allow for internal calibration, samples were measured in random order with frequent checks of the energy scale against the tabulated absorption edge energy of ruthenium foil to avoid systematic errors. The samples were placed in the *in situ* electrochemical cell with an optical path length of 50 mm. Absorption by the Mylar windows is negligible at the high energies used.

Data analyses were performed by using standard procedures for pre-edge subtraction, spline fitting and removal, and Fourier transformation.[32] Data were modeled in the curved wave approximation in *k*-space using theoretical amplitude functions as calculated by the computer program FEFF5.[33−35] These parameters were checked by fitting the known structures of tris(acetylacetato)ruthenium(III)[36] and ruthenium(IV) oxide.[37] The mean free path and coordination numbers were fixed in the final refinements.

Results and Discussion

Electrochemistry. The cyclic voltammograms of **1** using the *in situ* cell in a 0.5 M tetrabutylammonium hexafluorophosphate solution in acetonitrile in the absence and presence of an equimolar amount of TsOH are shown in Figure 3. Analogous results were obtained for the sample **2**. The two reduction waves shift toward more positive potential upon addition of the acid. The observed redox potentials are summarized in Table 1. The shift in the positive direction of the two reduction waves of **1** and **2** upon addition of TsOH is interpreted as a protonation of the oxo bridge in the oxidation states $Ru^{II}Ru^{II}$, $Ru^{II}Ru^{III}$, and $Ru^{III}Ru^{III}$, hereafter designated as $Ru^{II}Ru^{II}H$, $Ru^{II}Ru^{III}H$, and $Ru^{III}Ru^{III}H$, respectively. The protonation must occur at the $Ru^{III}Ru^{III}$ state, since the solution changes its color from blue to red upon addition of TsOH for both **1** and **2**. The present results with the *in situ* cell are consistent with the results previously reported for the samples with a standard electrochemical cell.[27]

Table 1. Redox Potentials vs Ag/AgCl for Samples **1**−**2**H in 0.5 M $(TBA)PF_6$ Acetonitrile Solution[a]

sample	$Ru^{II}Ru^{II}/Ru^{II}Ru^{III}$	$Ru^{II}Ru^{III}/Ru^{III}Ru^{III}$	$Ru^{III}Ru^{III}/Ru^{III}Ru^{IV}$
1	−1.09	−0.39	+0.95
2	−1.16	−0.55	+0.78
1 + TsOH	−0.10	+0.44	+0.96
2 + TsOH	−0.12	+0.29	+0.90

[a] TsOH = *p*-toluenesulfonic acid added in an amount equal to that of the diruthenium complex.

XAFS. The electric potentials for **1** (and **2**) applied to generate $Ru^{II}Ru^{III}$ and $Ru^{III}Ru^{IV}$ were −0.6 (−0.75) and 1.2 (1.0) V, respectively, and those for $Ru^{II}Ru^{II}H$ and $Ru^{II}Ru^{III}H$ were −0.45 (−0.5) and 0.15 (0.0) V against Ag/AgCl, respectively. The potential was kept at least for 3 h to ensure complete oxidation or reduction of the species. The Ru K-edge spectra of **1** at various oxidation states for both the μ-oxo and the μ-hydroxo forms are shown in Figure 4. The shape of the Ru K-edges is practically identical for all samples. This indicates that no major geometrical change occurs around the ruthenium atoms. Two clear trends can be seen in the shifts in energy of the absorption edges. First, the edge shifts slightly toward higher energy upon oxidation of the sample. The same trend was observed for all samples, including those in the presence of the acid. Second, the edge shifts to lower energy upon addition of TsOH to the sample, thus suggesting that the protonation at the oxide bridge causes the shift of the edge toward lower energy. These trends are consistent with what would be expected: Removal of electron(s) from the ruthenium by oxidation would increase the absorption edge energy, and protonation of the oxo bridge would reduce the electron density at the metal center.

Extracted EXAFS functions for **1** are shown in Figure 5, and the corresponding Fourier transforms in Figure 6. The obtained structural parameters are summarized in Table 2. Although the EXAFS spectra were refined fairly well, the final *r*-values are high. The main reason for this is the low signal in the EXAFS; the ruthenium accounts for only about one-third of the total absorption, the main absorber being the solvent. In order to achieve complete reduction or oxidation of the species electrochemically, the concentrations of the samples had to be kept low. In EXAFS experiments, on the other hand, a higher concentration is preferable, and a suitable compromise has to be sought. The ruthenium concentration used was thus 20 mM.

The largest peak in the Fourier transform of the EXAFS function represents the $Ru-O_{bridge}$, $Ru-O_{acetate}$, and $Ru-N_{ligand}$ distances, and the second largest peak mostly the ruthenium−ruthenium distance. Only in some cases was it possible to resolve the $Ru-O_{bridge}$ distance from the $Ru-O_{acetate}$ and $Ru-N_{ligand}$ distances due to a too small difference in the distances and the neighboring atomic numbers of O and N; the $Ru-O_{acetate}$ and $Ru-N_{ligand}$ distances had to be treated as one nitrogen shell in the analysis. The corresponding data of **1** and **2** in Table 2 are in good agreement with each other. The Ru···Ru distance are in reasonably good agreement with those determined by X-ray crystallography for the μ-oxo $Ru^{III}Ru^{III}$, μ-oxo $Ru^{III}Ru^{IV}$, and the μ-hydroxo $Ru^{III}Ru^{III}$ complexes (see Table 2). It is clear that the ruthenium−ruthenium distances decrease with decreasing formal oxidation state of the ruthenium atoms. This is interpreted as a decreased electrostatic repulsion between the ruthenium atoms. At the same time the $Ru-O_{bridge}$ distance increases, interpreted as a decreased electrostatic attraction between the ruthenium and bridging oxygen atoms. The $Ru-O_{acetate}$ and $Ru-N_{ligand}$ distances remained the same, within the error limit of the analysis, and a dependence on the ruthenium

(30) Nomura, M.; Koyama, A. In *X-ray Absorption Fine Structure*; Hasnain, S. S., Ed.; Ellis Horwood: London, **1991**; p 667.
(31) Nomura, M.; Koyama, A. Performance of BL10B and a simple performance test for EXAFS stations, KEK Report 89-16, 1989.
(32) Koningsberger, D. C.; Prins, R. *X-Ray Absorption-Principles, Applications, Techniques of EXAFS, SEXAFS and XANES*; John Wiley & Sons: New York, 1988.
(33) Mustre de Leon, J.; Rehr, J. J.; Zabinsky, S. I.; Albers, R. C. *Phys. Rev. B* **1991**, *44*, 4146.
(34) Rehr, J. J.; Albers, R. C.; Zabinsky, S. I. *Phys. Rev. Lett.* **1992**, *69*, 3397.
(35) Rehr, J. J.; Mustre de Leon, J.; Zabinsky, S. I.; Albers, R. C. *J. Am. Chem. Soc.* **1991**, *113*, 5135.
(36) Chao, G. K.-J.; Sime, R. L.; Sime, R. J. *Acta Crystallogr.* **1973**, *B29*, 2845.
(37) Armstrong, W. H.; Spool, A.; Papaefthymiou, G. C.; Frankel, R. B.; Lippard, S. J. *J. Am. Chem. Soc.* **1984**, *106*, 3653.

Table 2. Structural Parameters for Samples **1**−**2**H Obtained from the XAFS Analysis with Parameters from Crystal Structures of Similar Compounds (**A** and **B**, Oxo- and Hydroxo-Bridged, Respectively; See Footnotes) Included for Comparison[a]

		Ru−O_{bridge}				Ru−$(N,O)_{ligand}$				Ru−Ru				
sample	oxidn state	R (Å)	N	ΔE_0 (eV)	$10^2\sigma$ (Å^2)	R (Å)	N	ΔE_0 (eV)	$10^2\sigma$ (Å^2)	R (Å)	N	ΔE_0 (eV)	$10^2\sigma$ (Å^2)	r-factor[d]
1	$Ru^{II}Ru^{III}$					2.09	6	9.71	4.86	3.26	1	−14.6	6.98	0.32
	$Ru^{III}Ru^{III}$	1.89	1	14.0	4.01	2.08	5	14.0	4.24	3.28	1	−2.10	5.73	0.33
	$Ru^{III}Ru^{IV}$	1.82	1	4.54	3.43	2.08	5	4.54	3.43	3.36	1	2.15	4.56	0.30
2	$Ru^{II}Ru^{III}$					2.05	6	13.4	5.96	3.24	1	1.5	9.16	0.32
	$Ru^{III}Ru^{III}$	1.89	1	14.0	4.01	2.08	5	14.0	4.24	3.28	1	−2.10	5.73	0.33
	$Ru^{III}Ru^{IV}$	1.83	1	15.1	5.61	2.07	5	15.1	2.11	3.36	1	3.9	1.60	0.33
A	$Ru^{III}Ru^{III}$	1.864[b]	1			2.090[b]	5			3.266[b]	1			
	$Ru^{III}Ru^{IV}$	1.810[b]	1			2.053[b]	5			3.326[b]	1			
1 + TsOH	$Ru^{II}Ru^{II}$					2.07	6	5.00	5.40	3.37	1	29.7	12.9	0.31
	$Ru^{II}Ru^{III}$					2.07	6	7.40	4.63	3.31	1	28.8	9.23	0.30
	$Ru^{III}Ru^{III}$					2.05	6	8.04	4.78	3.54	1	9.07	8.62	0.35
2 + TsOH	$Ru^{II}Ru^{III}$					2.05	6	15.3	4.90	3.27	1	8.5	8.06	0.33
	$Ru^{III}Ru^{III}$					2.04	6	15.0	3.37	3.48	1	7.6	2.93	0.35
B	$Ru^{III}Ru^{III}$	1.98[c]	1				5			3.472[c]	1			

[a] R, N, ΔE_0, and σ represent the interatomic distance, the coordination number, the shift in photoelectron energy zero, and the Debye−Waller factor, respectively. [b] Crystallographic data of **1** taken from ref 11. [c] Crystallographic data $Ru_2(\mu\text{-OH})(\mu\text{-CH}_3\text{COO})_2$(1,4,7-trimethyl-1,4,7-triazacyclononane)$_2(ClO_4)_3$ taken from ref 10. [d] $r = [\sum k^6\{\chi_{obs}(k) - \chi_{calc}(k)\}^2/\sum k^6\chi^2_{obs}(k)]^{1/2}$. The uncertainties in interatomic distances in the first and the outer shells are ±0.02 and ±0.05 Å respectively.

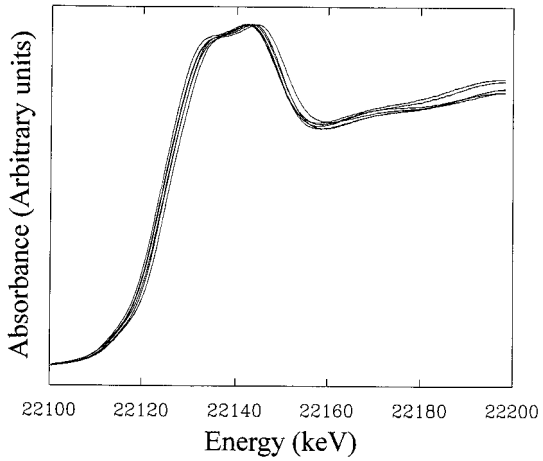

Figure 4. XANES spectra of the different oxidation states of **1** and **1** + TsOH. The six spectra from the lower energy side correspond to the oxidation states of diruthenium, (II,II H), (II,III H), (II,III), (III,-III), (III,III H), and (III,IV).

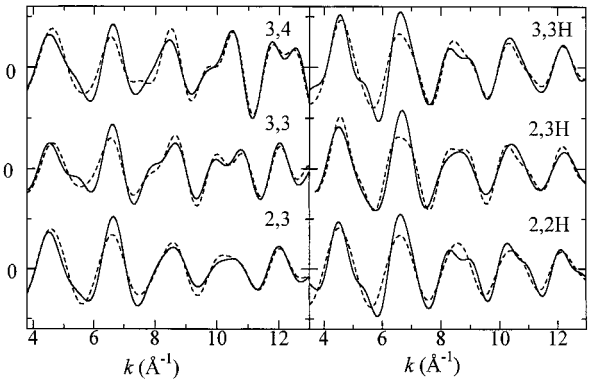

Figure 5. k-weighted EXAFS functions, $\chi(k)\cdot k^3$, of the different oxidation states of **1** and **1** + TsOH. The solid lines are experimental values, and the dashed lines are those based on the models given in Table 2.

oxidation state was not experimentally observed. The overall change in shape is thus an opening of the Ru−O_{bridge}−Ru bond angle.

The ruthenium−ruthenium distance increases as the oxo bridge is protonated to the corresponding hydroxo-bridged complexes. This trend has often been observed for complexes with the $M_2(\mu\text{-O(H)})(\mu\text{-RCOO})_2$ core, such as M = Fe^{III} (3.120 to 3.439 Å)[37,38] and M = Mo^{III} (2.885 to 3.555 Å).[39] The differences (ΔR) in metal−metal distance between the oxo- and hydroxo-bridged complexes are 0.319 and 0.670 Å for the Fe^{III} and Mo^{III} complexes, respectively. In the latter case, it has been suggested that the direct molybdenum−molybdenum bond formed in the μ-oxo complex is broken upon protonation at the oxide bridge, resulting in a longer molybdenum−molybdenum distance. In the present study the ΔR values are 0.26 and 0.05 Å for the $Ru^{III}Ru^{III}$ and $Ru^{II}Ru^{III}$ states of **1** and 0.20 and 0.03 Å, respectively, for **2**. A very small ΔR for the $Ru^{II}Ru^{III}$ state is noteworthy. A similarly small ΔR value has been reported for $V^{III}V^{III}$ complexes,[40] interpreted as a result of the d^2 electron configuration of V^{III} which does not prefer the bent V−O−V structure, although the reason for the small ΔR value for the $Ru^{II}Ru^{III}$ is not clear at present; the charge localization−delocalization of the mixed-valence state might be involved.

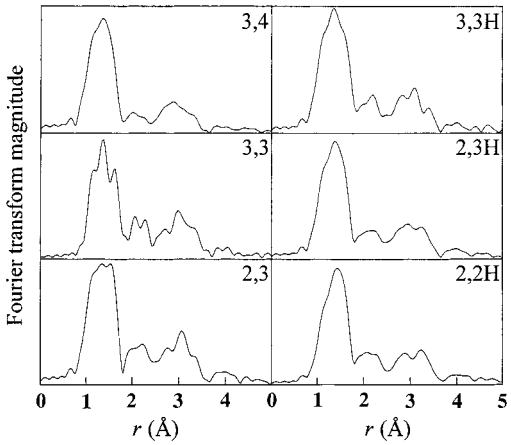

Figure 6. Fourier transforms of the different oxidation states of **1** and **1** + TsOH.

Within the series of the Ru_2 oxidation states $Ru^{II}Ru^{II}H$, Ru^{II}-$Ru^{III}H$, and $Ru^{III}Ru^{III}H$, with hydroxo bridges, the $Ru^{II}Ru^{III}$ complex has the shortest ruthenium−ruthenium distance. Previ-

(38) Hartman, J. R.; Rardin, R. J.; Chaudhuri, P.; Pohl, K.; Wieghardt, K.; Nuber, B.; Weiss, J.; Papaefthymiou, G. C.; Frankel, R. B.; Lippard, S. J. *J. Am. Chem. Soc.* **1987**, *109*, 7387.
(39) Neves, V. A.; Bossek, U.; Wieghardt, K.; Nuber, B.; Weiss, J. *Angew. Chem., Intl. Ed. Engl.* **1988**, *100*, 718.
(40) Bond, M. S.; Czernuszewicz, R. S.; Dave, B. C.; Yan, Q.; Mohan, M.; Verastegue, R. and Carrano, C. J. *Inorg. Chem.* **1995**, *34*, 5887.

ously reported μ-hydroxo dimers have often shown that the metal−metal distance decreases upon lowering the oxidation states, e.g. 3.400 Å for $[Fe^{II}Fe^{III}(\mu\text{-OH})(\mu\text{-pivalate})_2(Me_3tacn)_2]^{2+}$, 3.439 Å for $[Fe^{III}Fe^{III}(\mu\text{-OH})(\mu\text{-CH}_3COO)_2(HBpz)_2]^{+}$, and 3.32 Å for $[Fe^{II}Fe^{II}(\mu\text{-OH})(\mu\text{-CH}_3COO)_2(Me_3tacn)_2]^{+}$.[7,41,42] However, there is also an exceptional case for $Ru^{II}Ru^{II}(\mu\text{-OH}_2)(\mu\text{-C}_6H_5COO)_2(MeCN)_2(O_2CAr)_2(PPh_3)_2$ and $Ru^{II}Ru^{III}(\mu\text{-OH}_2)(\mu\text{-C}_6H_5COO)_2Cl(MeCN)(O_2CAr)_2(PPh_3)_2$, in which the ruthenium−ruthenium distances are 3.712 and 3.604 Å, respectively.[15] The value of 3.604 Å is longer than that of the $Ru^{II}Ru^{III}H$ hydroxo complex as expected from further protonation at the hydroxo bridge. It has been reported that the μ-aqua $Ru^{II}Ru^{III}$ complex has a spin-trapped delocalized state as verified by X-ray structural analysis. It is thus interesting to know whether the hydroxo-bridged, mixed-valence state of **1** is in a spin-trapped or delocalized electron structure.

Conclusions

The *in situ* XAFS measurements with the electrochemical cell have revealed the structural parameters, in particular, the ruthenium−ruthenium distances of the oxo- or hydroxo-bridged ruthenium dimers $[Ru_2(\mu\text{-O(H)})(\mu\text{-CH}_3COO)_2(bpy)_2L_2]^{n+}$ in the oxidation states from (II,II) to (III,IV) in acetonitrile solution. The decreased oxidation state of the ruthenium atoms is reflected in the absorption edge positions, which shifts to lower energy upon reduction and/or protonation of the μ-oxo bridge. The ruthenium−ruthenium distances decrease with decreasing ruthenium oxidation states for the oxo- and hydroxo-bridged complexes, except for the hydroxo-bridged $Ru^{II}Ru^{III}$ species, which has an unusually short ruthenium−ruthenium distance. This structural information will be useful in considering structural changes of the binuclear metal center of metalloenzymes during catalytic processes.

Acknowledgment. This work was performed under the approval of the Photon Factory Program Advisory Committee (Proposal No. 94G015) and partly supported by the Ministry of Education, Science, and Culture (Grant Nos. 6453029, 8640656, and 9440207).

IC970339V

(41) Armstrong, W. H.; Lippard, S. J. *J. Am. Chem. Soc.* **1984**, *106*, 4632.

(42) Hartman, J. R.; Rardin, R. L.; Chaudhuri, P.; Wieghardt, K.; Nuber, B.; Weiss, J.; Papaefthymiou, G. C.; Frankel, R. B.; Lippard, S. J. *J. Am Chem. Soc.* **1987**, *109*, 7387.